A critical evaluation of copper isotopes in Precambrian Iron Formations as a paleoceanographic proxy

Fanny Thibon, Janne Blichert-Toft, Francis Albarède, John Foden, Harilaos Tsikos

A critical evaluation of copper isotopes in Precambrian Iron Formations as a paleoceanographic proxy

Fanny Thibon[a], Janne Blichert-Toft[a*], Francis Albarede[a], John Foden[b], and Harilaos Tsikos[c]

[a]*Laboratoire de Géologie de Lyon, Ecole Normale Supérieure de Lyon, CNRS UMR 5276, Université de Lyon, 46 Allée d'Italie, 69007, Lyon, France*

[b]*Geology and Geophysics, School of Earth and Environmental Sciences, University of Adelaide, Adelaide, SA 5005, Australia*

[c]*Geology Department, Rhodes University, Grahamstown 6140, South Africa*

*Corresponding author: jblicher@ens-lyon.fr; +33608134849

Abstract

Trace metals in Iron Formations (IF) have been widely used as proxies for oceanic redox processes and oxygen evolution leading to the Great Oxidation Event (GOE). Copper has hitherto received comparatively little attention, with a single study reporting variation in δ^{65}Cu between pre- and post-GOE black shales. This is attributed to postulated isotope fractionation effects in the pre-GOE ocean during widespread iron oxide deposition in IF. Here we focus on the application of Cu isotopes in two classic IF-containing sequences of the Neoarchean-Paleoproterozoic, namely the Hamersley (Australia) and Transvaal (South Africa) Supergroups. We specifically targeted the oxide-rich Joffre and Kuruman IF, the carbonate-rich Griquatown IF, and the Mn-rich Hotazel IF, which collectively record over 100 Ma of sustained IF deposition in the pre-GOE ocean. The aim was to assess the utility of Cu isotopes

in IF as a paleoceanographic proxy in view of existing oxygen evolution models. Iron formation Cu concentrations are low compared to average crust and modern oceanic Fe-Mn oxide deposits, with average values between 1 and 5 ppm for all four IF data sets. Copper concentrations show no systematic variability with mineralogy, no statistical correlation with bulk Fe and Mn contents, good correlations with Ti (r_{Cu-Ti} = 0.73) for the Joffre data set and with Cr, Ni, and V for the South African data sets, and shale-like Cu/Ti ratios. Isotopic results show statistically invariant average δ^{65}Cu values very close to 0 ‰ for all but the Joffre IF which has a marginally negative average δ^{65}Cu value (-0.24 ± 0.22 ‰). Combined with other trace transition metal systematics, the Cu isotope data point to a Cu source that was controlled largely by inputs of fine volcanic-derived particles (ash), thus placing limitations on its utility as a paleoceanographic redox proxy during IF genesis.

Keywords

Iron formation; Great Oxidation Event; Copper isotopes; Ocean chemistry; Transvaal Supergroup; Hamersley Supergroup

1. Introduction

The concentrations and stable isotope ratios (where applicable) of trace metals in Precambrian marine sedimentary rocks (iron formations-IF, carbonates, black shales) and paleosols have been variously utilised as key records for the reconstruction and redox evolution of the marine and terrestrial realms of the early Earth (Anbar and Rouxel, 2007). Constraints on a Neoarchean onset of oxygenic photosynthesis have been gleaned from the

isotopic records of several redox-sensitive elements such as Mo (e.g. Planavsky et al. (2014)), Cr (Crowe et al., 2013), and, more recently, U (Wang et al., 2018), and Tl (Ostrander et al., 2019). The use of Cr fractionation as a proxy of Mesoarchean oxidative weathering has, however, been questioned because of uncertain preservation of the rocks (Albut et al., 2018). Complementing the isotopic record is a number of independent studies applying trace metal geochemistry which has further illuminated the processes and effects leading to the first appearance of oxygen in the atmosphere, the so-called Great Oxidation Event (GOE). Konhauser et al. (2009) used declining molar Ni/Fe ratios in IF, while Swanner et al. (2014) focused on secular variations in Co abundance in marine shales and IF, in both instances as tracers of oxygen evolution through time. Similar constraints on the GOE have been provided through the U record of IF (Partin et al., 2013), the Zn/Fe ratio of marine carbonates (Liu et al., 2015b), and the Cu isotopic record of marine black shales (Chi Fru et al., 2016). Proxies for oxidative weathering in the Archean prior to the GOE include Mo and Re concentrations, and Re/Mo ratios in marine shales (Anbar and Rouxel, 2007; Kendall et al., 2010; Scott et al., 2008; Sheen et al., 2018), and Cr isotopes in IF and paleosols alike (Crowe et al., 2013; Frei et al., 2016; Frei et al., 2011).

In terms of Precambrian IF, the fundamental premises for the use of a given trace metal as a reliable proxy for water-column processes is that the residence time of the element in question in the ocean is long enough with respect to the time interval averaged by the sample size or that multiple coeval sedimentary pathways compete for the sedimentary output. From the record of Fe isotopes in pre-GOE IF drill cores, Thibon et al. (2019) demonstrated that Fe has a residence time in the Archean ocean in the million year range, which makes Fe a good redox paleoproxy. Iron formations are widely thought to represent the products of primary, cyclic marine iron oxyhydroxide and silica precipitation (Posth et al., 2008) that was

subsequently transformed into the present assemblages, mainly through diagenetic bacterial iron reduction (e.g. DIR) (Heimann et al., 2010). Diagenesis would have produced predominantly ferrous assemblages from the ferric precursors in the presence of an electron donor, a role widely thought to have been played by co-precipitated organic matter (Konhauser et al., 2017). Ferrous minerals in IF are mainly carbonates and silicates of iron, with magnetite essentially being the chief Fe(III) host (Oonk et al., 2017). Therefore, in principle, the more iron carbonate and silicate-rich an IF is, the more diagenetically modified it is from the original oxyhydroxide precursor. Consequently, carbonate-silicate facies IF may have been the comparatively more likely candidates for open-system fractionation effects during diagenesis, with high potential for alteration of their primary signals in absolute concentrations and stable isotope ratios of contained trace metals.

It follows that for trace metal concentrations and stable isotope ratios to work as effective proxies, the assumption has to be made that diagenesis would have operated as a closed system with respect to the elements of choice. Alternatively, the water-column isotope ratio signature must have been fortuitously retained in the sediment during open system diagenetic transformations. For closed system conservation of isotopic signals to have occurred, the added condition would be that either the trace metals formed discrete authigenic mineral phases stable under the new conditions, or they systematically and quantitatively entered the structure of newly-formed mineral phases that dominate the composition of IF, such as magnetite, iron carbonates, and iron silicates (Oonk et al., 2017).

A recently introduced complexity with respect to partly or wholly reduced Fe minerals in IF is the growing body of evidence that some of them may have formed as primary precipitates under high oceanic alkalinity in the form of greenalite (Johnson et al., 2018) or magnetite

(Thibon et al., 2019). Primary precipitation of such minerals means that sequestration and isotopic fractionation of associated trace metals would be guided in each case by correspondingly distinct physico-chemical principles and parameters, which may differ markedly from those pertaining to ferric oxyhydroxide nucleation and precipitation. Here, we will employ the traditionally prevailing view in the published literature that the sedimentary precursor in IF was predominantly ferric oxyhydroxide (such as ferrihydrite; Konhauser et al. (2007)). This would occasionally have been accompanied by co-precipitation of Mn(IV) oxides, which presumably would have been driven by transient periods of increased redox potential in the ocean (e.g. "oxygen whiffs"; see Anbar et al. (2007); Kurzweil et al. (2016)).

Copper is arguably one of the metals that has received the least attention as a redox proxy for Paleoproterozoic oceanography. To the best of our knowledge, there are hitherto no published studies utilising Cu and its isotopes in IF. The recent study by Chi Fru et al. (2016) is the only work that focuses on Cu isotopes as a record of the GOE, albeit entirely on results from black shales deposited before and after the GOE. Nevertheless, Chi Fru et al. (2016) postulate global IF deposition in the pre-GOE ocean as a driver for effective sequestration of isotopically heavy Cu (^{65}Cu) out of seawater, by virtue of the expected positive fractionation effect linked to the sorption of Cu onto precursor ferric oxyhydroxides (Balistrieri et al., 2008). The resultant reservoir effect in terms of negative Cu isotope fractionation in the oceans would have been quantitatively captured in pre-GOE black shales. At post-GOE times, paucity of IF deposition along with corresponding changes in sources and sinks of Cu in the terrestrial and marine environments would have resulted in black shale deposition recording positive values of $\delta^{65}\mathrm{Cu} = \left[\frac{\left(^{65}\mathrm{Cu}/^{63}\mathrm{Cu}/\right)_{sample}}{\left(^{65}\mathrm{Cu}/^{63}\mathrm{Cu}/\right)_{NIST\,976}} - 1\right]$.

NIST 976 stands for the isotopic Standard Reference Material (SRM) (copper metal) provided by the National Institute of Standards and Technology (NIST). In this work, we provide the first comprehensive record of the Cu isotopic composition of four major IF sequences from the Transvaal and Hamersley Supergroups in South Africa and Australia, respectively, that span over 100 million years of chemical iron deposition immediately before the GOE. We critically assess our results against the broader mineralogical and geochemical characteristics of the examined IF, and provide constraints on the sources and sinks of Cu during deposition and diagenesis. We then evaluate the potential of Cu isotopes for constraining redox processes in the pre-GOE ocean through time, in light of both existing models and in more general terms. Finally, we highlight some of the caveats in the wider application of trace metal geochemistry of IF as a paleoenvironmental proxy, especially when the speciation and mineralogical distribution of these metals in the primary sedimentary environment are neither adequately understood nor rigorously constrained.

2. Samples and analytical techniques

Four drill cores capturing representative sections of IF from the Transvaal Soupergroup of South Africa and the Hamersley Supergroup of Australia were sampled for the purpose of this work. Detailed information on the geological settings and full descriptions of the samples are given in the Electronic Supplement of Thibon et al. (2019). The three South African drill cores, referred to as GAS, LO1, and MP56, capture, respectively, the Kuruman, Griquatown, and Hotazel IF, which collectively span the time interval between 2521 and 2394 Ma (Gumsley et al., 2017). The fourth drill core, GW, from Hamersley captures part of the Joffre member of the Brockman IF, which has been dated at 2463 to 2449 Ma (Pickard, 2002). The IF deposition

rates have been independently assessed by U-Pb chronology and Co deposition rates (Thibon et al., 2019). The rates of 4-30 m/Ma obtained by the two methods are consistent and have received further support from the comparison of stratigraphy with orbital periods (Lantink et al., 2019).

One of the issues associated with laminated samples is the chemical variability induced by mineral grain size and banding. A total of 156 samples were collected from the four drill cores in the form of 10 to 20 cm-long quartered cores every one to five meters on average along the entire length of each core (MP56: 362.46-458.80 meters depth; LO1: 122.35-355.60 meters depth; GAS: 0-522.70 meters depth; GW: 40-101 meters depth). The length was chosen to correspond to a moving average, or, equivalently, to a low-pass filter, removing fluctuations shorter than about 10,000 years. Unfortunately, the range of variations of Cu isotopes is too small to apply the technique of Thibon et al. (2019) for determining the Cu oceanic residence time. Thibon et al. (2019) also reported Fe isotope data on samples from the LO1 core collected on the cm-scale. Although the major and trace element and Fe isotopic compositions of these centimetric samples averaged over 10-20 cm are fully consistent with the values obtained on the corresponding decimetric samples, they are significantly noisier. We therefore concluded that short-range fluctuations reflect mineral abundances and, hence, for the remainder of the study focused on the decimetric samples collected every 10 to 20 cm along the cores.

Each sample was crushed into small fragments and approximately a quarter of each was pulverized into fine powder in order to provide a bulk average of the sample mineralogy on a 10 to 20 cm length scale. Approximately 100 mg of sample powder for each sample was digested in concentrated distilled HF:HNO_3, evaporated to dryness, then redissolved in

concentrated distilled 3:1 HCl:HNO_3 (*aqua regia*). After another round of evaporation to dryness, the samples were taken up in 6 M HCl. Two aliquots were prepared: the first aliquot, consisting of 5% of the sample solution, was dedicated to elemental analyses; the second aliquot (i.e. the remaining 95% of the sample) was dedicated to Cu isotopic measurements. A key requirement for the latter is the elimination of most of the iron of the sample solution as it will otherwise saturate the resin used for copper purification. Copper, therefore, was first eluted with the sample matrix using 25 mL of 4 M HCl on a column filled with 3mL AG1-X8 resin, while >90% of the Fe was retained on the column. Copper was then separated from the sample matrix and remaining Fe following the procedure of Maréchal et al. (1999), which uses 1.8 mL of AG-MP1 resin and 7 M HCl with 0.001 % H_2O_2. Further details of the chemical purification protocol, yields, blanks, and reference values can be found in Maréchal et al. (1999) and a number of later references from several groups who adopted the "Maréchal" Cu separation procedure.

Elemental concentration analyses were done on a Thermo-Scientific ICAP ICP-OES for major elements and a Thermo-Scientific ELEMENT2 ICP-MS for minor and trace elements, both at the Ecole Normale Supérieure de Lyon (ENS de Lyon). The analyses followed a 22-sample batch procedure with each batch containing 20 samples (unknowns), the IF reference material IF-G, and a blank, the latter two of which had been through all the same steps as the samples so as to provide measures of the total procedural blank and the reproducibility of the technique. All eight total procedural blanks fell below the level of detection for all elements analysed. The mean external reproducibility of the IF-G reference material was ~10% for major element concentrations and ~30% for minor and trace element concentrations. Most of this variability is ascribed to the inherent heterogeneity of the reference material itself.

Our elemental measurements are in excellent agreement with the published values of Govindaraju (1995) (see Electronic Supplement, Fig. S1).

Copper isotopic compositions were measured on a Nu Instrument 500 HR MC-ICP-MS, also at ENS de Lyon. Again, all eight total procedural blanks for Cu fell below the level of detection. Samples and standards (SRM NIST 976) were analyzed in wet plasma conditions in low-resolution mode (R ~ 300) with SRM NIST 976 run systematically every two samples. With optimal Cu purification as described above, low-resolution mode is sufficient to resolve all Cu interferences (Xe^{++}, Te^{++}, $^{31}P^{16}O_2^+$, $^{40}Ar^{23}Na^+$, and $^{47}Ti^{16}O^+$ for ^{63}Cu, and Xe^{++}, Te^{++}, Ba^{++}, $^{49}Ti^{16}O^+$, $^{40}Ar^{25}Mg^+$, $^{32}S^{33}S^+$, $^{32}S^{16}O^{17}O^+$, $^{33}S^{16}O_2^+$, and $^{31}P^{16}O^{18}O^+$ for ^{65}Cu). The optimum Cu concentration for isotopic measurement is 0.3 mg/L, which gives a maximum intensity of 3V of Cu, but concentrations down to 0.05 mg/L are acceptable in good running conditions. Instrumental mass bias correction was done by combining external correction (i.e. sample-standard bracketing using SRM NIST 976) with internal correction using the exponential fractionation law applied to a Zn solution added to both the samples and bracketing standards. The mean value and reproducibility of 19 replicate measurements of the IF-G reference material typically used in IF geochemical studies gave $\delta^{65}Cu_{IFG} = -0.23 \pm 0.20$ ‰ (2σ). Precision, therefore, is 0.10 ‰ per amu. To the best of our knowledge, no other $\delta^{65}Cu_{IFG}$ measurements of this reference standard material have been published so far.

3. Results

Bulk-rock major, minor, and trace element data and $\delta^{65}Cu$ values of all samples, accompanied by tabulated correlation coefficients for each of the four IF sample sets analysed, are archived in the Electronic Supplement (Tables S1 and S2). The elemental data were previously

208 published in Thibon et al. (2019), but for the reader's convenience we include them here as
209 well. In general, the mineralogy and bulk geochemistry of the targeted IF have recently been
210 studied or reviewed comprehensively (Joffre IF: Haugaard et al. (2016); Kuruman/Griquatown
211 IF: Oonk et al. (2017); Hotazel IF: Tsikos et al. (2003); Tsikos et al. (2010)). Hence, the main
212 emphasis in this section will be placed on the behavior of Cu, both its abundances and its
213 isotopic compositions, in connection with the gross mineralogical and geochemical
214 characteristics of the rocks.

215 One of the geochemical parameters that provides a close approximation of the modal
216 mineralogy for all IF is the bulk average Mn/Fe ratio, multiplied here for convenience by a
217 factor of 10^3 and hereinafter referred to as Mn*/Fe. As previously demonstrated, Mn in at
218 least the South African IF is hosted almost exclusively (>90%) in the carbonate fraction and
219 specifically in the minerals siderite and ankerite in the Kuruman and Griquatown IF (Oonk et
220 al., 2017) and in kuthahorite and Mn-calcite in hematite lutites of the Hotazel IF (Tsikos et al.,
221 2003). By contrast, Fe is contained dominantly in the mineral magnetite (and hematite in the
222 case of the Hotazel hematite lutite samples), although a fraction of the bulk Fe is also
223 invariably contained in the aforementioned carbonate minerals and in iron silicate species.
224 The parameter Mn*/Fe can therefore effectively serve as the approximate ratio of bulk
225 carbonate *versus* bulk oxide in IF, while at the same time constituting a measure of the relative
226 role of Mn *versus* Fe on the speciation of trace metals such as Cu.

227 Based on the Mn*/Fe ratio, the selected IF sample sets complement each other well in terms
228 of bulk mineralogy and geochemistry (Fig. 1a): the Joffre IF is the most oxide (magnetite)-rich
229 member, with a Mn*/Fe ratio of 4.2, while the slightly more carbonate-rich Kuruman IF has a
230 Mn*/Fe ratio of 8.4. The Griquatown IF is the most carbonate (ankerite+siderite)-rich

231 member, with a bulk Mn*/Fe ratio of 24.8. The Hotazel IF sample set has a far more
232 heterogeneous composition as it comprises Mn-poor, magnetite+Fe carbonate facies IF, as
233 well as a manganese carbonate-rich sub-facies containing abundant hematite (hematite
234 lutite). This compositional heterogeneity gives rise to an exceptionally high average Mn*/Fe
235 ratio of 317. Exclusion of the hematite lutite samples still results in a high mean Mn*/Fe of
236 46.1.

237 The concentration of Cu in the samples from the Transvaal Supergroup IF is low and compares
238 well with literature data, ranging between 1 and 10 ppm for >95% of all samples analysed.
239 There is, however, no statistical correlation between average Cu abundance from each IF and
240 bulk-rock Fe, bulk-rock Mn, or the ratio thereof, with correlation coefficients always lower
241 than 0.3. When average bulk-rock Cu values are normalised to bulk average Fe for each
242 sample set, the only notable relationship that emerges is a subtle increase in the ratio of
243 $Cu*10^6/Fe$ (hereinafter referred to as Cu*/Fe) from the Joffre IF (13.9), to the Kuruman IF
244 (14.9) and ultimately the Griquatown IF (18.8) (Fig. 1b). This relationship is crudely correlated
245 with the increasing Mn*/Fe ratio across these three IF sample suites, pointing to a broadly
246 inverse relationship between bulk Fe and Cu.

247 Contrary to the aforementioned lack of correlation between Cu and Fe or Mn, each IF displays
248 its own weak to moderate positive correlations of Cu with other major and/or trace elements,
249 and specifically with transition metal concentrations (Fig. 2). In the Transvaal IF sample sets,
250 correlation coefficients between Cu and Ni, Cr, and V (Figs. 2a-c) are – with one single
251 exception – higher than 0.5, with the highest values observed in the Kuruman formation data
252 set (Table 1). By contrast, Cu concentrations in the Joffre IF correlate well with Ti, with a
253 correlation coefficient of 0.73. This is in agreement with previously published Ti and Cu

concentration data of the Joffre IF (Chi Fru et al., 2016), which show a correlation coefficient as high as 0.85 (Fig. 2d).

Copper isotope compositions are displayed in Fig. 1c. Copper isotope ratios exhibit very low variability within each IF, at a maximum standard deviation of $\pm$ 0.2 ‰. Specifically, the Joffre IF has average δ^{65}Cu = -0.24 $\pm$ 0.22 ‰; the Kuruman IF δ^{65}Cu = 0.02 $\pm$ 0.13 ‰; the Griquatown IF δ^{65}Cu = 0.01 $\pm$ 0.09 ‰; and the Hotazel IF δ^{65}Cu = -0.01 $\pm$ 0.12 ‰. It is evident from the above data that the Transvaal IF show no statistical difference in average δ^{65}Cu among the three data sets (p-value = 0.7) with average values extremely close to 0 ‰, whereas the Joffre IF has a statistically distinct and marginally lower δ^{65}Cu average value than those of the South African IF (p-value <0.001).

4. Discussion

4.1. Iron formations as a Cu sink

Copper and Fe variations are visibly decoupled (Fig. 3), which indicates that the two elements are controlled by different processes. The determination of Fe residence time (~2 Ma) in the Archean ocean by Thibon et al. (2019) is based on Fe isotopes and therefore is robust. Although Fe isotopes are a good paleoceanographic proxy, the same may not be the case for Cu isotopes. The lack of large δ^{65}Cu fluctuations in the present IF cores indicates that either Cu residence time in the ocean is <10,000 years (fast transfer from input to sediments, fluctuations averaged out) or input δ^{65}Cu did not change much over long time intervals.

An additional key parameter that would inform the utility of Cu and its stable isotopes as a palaeoceanographic proxy, but is hitherto unconstrained, is the average δ^{65}Cu of the Neoarchean-Paleoproterozoic oceanic Cu inventory. Given the uncertainties, we first

277 evaluate the abundance of Cu as registered in the bulk-rock composition of the IF analysed
278 here. In terms of average trace metal concentrations, all four IF data sets are clearly low with
279 respect to the average crust, and between one and three orders of magnitude lower than the
280 abundances recorded in Mn nodules in the modern ocean (with the single exception of Cr;
281 Fig. 4). The situation does not change in any major way when the concentrations of Cu are
282 considered as ratios against Fe (Cu/Fe=~10^{-5}, this work, *versus* 5x10^{-4}, Rudnick and Gao
283 (2003)). In their oceanic Cu model around the GOE, Chi Fru et al. (2016) postulate a relative
284 Cu/Fe sedimentation rate equivalent to approximately 1/4500 (Konhauser et al., 2002) which,
285 if multiplied by 10^6 for direct comparison with the Cu*/Fe parameter used earlier (Fig. 1),
286 would result in a value as high as 220. This value is at least an order of magnitude higher than
287 each of the average Cu/Fe ratios for the four IF analysed in this study.

288 Further insights into IF as an effective (or not) Cu sink can be derived from the use of Cu/Ti
289 ratios. Here, Cu concentrations are assessed against Ti, which is widely regarded as a proxy of
290 the terrigenous detrital fraction in marine sediments. A key postulate in previous studies (Chi
291 Fru et al., 2016) is that IF deposited prior to the GOE constituted a sustained and effective
292 oceanic Cu sink by comparison to black shale deposits. We have plotted our entire data set of
293 molar Cu/Ti ratios against time for our four selected IF (Fig. 5, adapted from Chi Fru et al.
294 (2016)), on the contention that our data represent two of the classic and most voluminous
295 pre-GOE IF sequences globally. Contrary to earlier suggestions of Chi Fru et al. (2016) that at
296 least the pre-GOE IF are relatively more enriched sedimentary Cu sinks than coeval black
297 shales, we observe that all four formation averages and >95% of the data plot well into the
298 black shale field. This clearly indicates that at least the IF targeted here were comparatively
299 no more or less important than organic-rich siliciclastic deposits in terms of net precipitation
300 of Cu in the primary sedimentary environment.

Understanding Cu behavior requires an assessment of its speciation in Archean seawater. Under the reducing conditions prevailing to maintain positive Eu anomalies, the redox potential of the environment must be negative (Danielson et al., 1992) and, therefore, Cu must be in its reduced form. In addition, Cu^{+} is strongly chelated by chlorine, notably $CuCl_3^{2-}$ (Dekov et al. (2013), Fig. 6), which reduces the sedimentary Cu output rate and makes the residence time of Cu dissolved in the ocean longer.

4.2. Sources and fate of Cu during IF deposition and diagenesis

The very low concentrations of Cu presented in this paper can be fundamentally explained either by much lower fluxes of Cu in association with primary Fe oxyhydroxide precipitation than postulated elsewhere (e.g. Konhauser et al. (2002)), and/or remobilisation of most of the deposited Cu and loss from the sediment during diagenetic recycling. Irrespective of the exact process or combination of processes, some further conclusions can be drawn from our new Cu isotope results in conjunction with selected bulk geochemical characteristics of the rocks in question.

In terms of average Cu isotope ratios, the Joffre IF has a marginally lower $\delta^{65}Cu$ value than the other three IF from South Africa. The positive correlation between Cu and Ti in Fig. 2d can be interpreted as an association with fine-grained clastic input from a terrigenous or volcanic source. This association is further supported by the comparable range of Cu/Ti values of the Joffre IF samples with those defining the shale field of Fig. 5. In the absence of any statistical correlation of Cu with bulk Fe, we propose that the Cu isotope signal captured in the Joffre IF is essentially the signal of co-precipitated Cu-bearing particles that are genetically unrelated to processes of primary Fe-oxyhydroxide precipitation out of the oceanic water column.

The situation with the Cu isotope signal of the three South African IF is somewhat less clear. The Kuruman IF is closely comparable to the Joffre IF in terms of the dominance of magnetite and low modal abundance of carbonate minerals. Assuming that magnetite is the compositionally closest diagenetic mineral to precursor ferric oxyhydroxide, our expectation is that it would have been the most likely candidate to retain primary Cu in the sediment during diagenesis. However, again there is no statistical correlation between Cu and bulk-rock Fe in the Kuruman IF; instead, there are strong positive correlations between Cu and Cr, Ni and V (Fig. 2). Previous studies on the trace metal speciation of the Kuruman and Griquatown IF (Oonk et al. (2017); see also Fig. 7) have indicated that Cr is associated with the IF detrital fraction and shows a good correlation with bulk-rock Zr. By extension, and in the absence of Zr measurements on our current samples, we are inclined to interpret the Cu isotopic signature of the Kuruman IF as also reflecting mainly the fine-grained clastic (i.e. non-chemical) fraction of the original sediment.

The Griquatown and Hotazel Formations add important additional dimensions not only with regard to the origin of Cu but also the fate of Cu during diagenetic processes. The Griquatown IF is thought to have been deposited in a relatively shallower environment (above wave base) than the Kuruman IF. It is therefore dominated by Fe carbonate minerals relative to magnetite, and it also has a marginally higher modal detrital component of a presumed terrigenous source (Oonk et al., 2017). Furthermore, the mean of Mn*/Fe and Cu*/Fe ratios of the Griquatown IF are clearly higher than those of the Kuruman IF. Previously published speciation results for Cu and other trace metals (Fig. 7) indicate that the carbonate and silicate mineral fractions are the main hosts for Cu, while Mn is almost entirely hosted in the carbonate fraction. Whereas the weakly positive correlation of Cu with Cr (Fig. 2a) suggests that some of the Cu is probably hosted in fine-grained particles of a non-chemical origin (as

for the Kuruman IF), a fraction of the Cu in the Griquatown IF may be associated with primary Mn oxide that is now recycled – partly or wholly – into Mn-rich iron carbonates during anaerobic diagenesis. Studies of Mn(IV)-rich deposits in the modern ocean (Little et al., 2014a; Little et al., 2014b) have demonstrated an affinity to the isotopically light Cu isotope (^{63}Cu). In view of this association, the increased Mn/Fe ratio in the Griquatown IF could be expected to record a relatively low δ^{65}Cu, certainly lower than seen in the Kuruman IF; this is, however, clearly not the case, as the δ^{65}Cu average of the Griquatown IF is statistically indistinguishable from that of the Kuruman IF.

The Hotazel sample set provides an even better candidate to assess the relative role of high primary fluxes of Mn in controlling primary Cu isotope variations. The selected Hotazel samples range from Mn-poor, magnetite+carbonate-rich IF to hematite-rich lutites with a high abundance of Mn in carbonate minerals, again widely interpreted to represent diagenetic products of MnO_2 reduction (Tsikos et al., 2003; Tsikos et al., 2010). The probability is high, therefore, that the Hotazel samples would capture low δ^{65}Cu signatures directly associated with elevated Mn/Fe ratios.

The potential for the Hotazel samples to record the lowest δ^{65}Cu signatures could in fact be augmented further for an additional reason: very low δ^{56}Fe data in the Hotazel IF have been previously interpreted as a highly evolved signature during Rayleigh fractionation of heavy Fe isotopes into Mn-poor BIF in the pre-GOE ocean (Tsikos et al., 2010). If the same principle is applied in the case of Cu and its isotopes, as also put forward by Chi Fru et al. (2016), then highly fractionated δ^{65}Cu ought to have been recorded in the most Mn-enriched portions of the Hotazel IF (i.e. lower than the Mn-poor samples). The essentially invariant δ^{65}Cu data across the entire Hotazel sample suite irrespective of the large variations displayed by Mn/Fe

371 suggests that, again, the anticipated low Cu isotope signal linked to putative primary MnO_2
372 deposition was either absent in the primary environment, or has been completely erased
373 during diagenetic mineral transformations. It therefore becomes increasingly likely that the
374 very close similarity between the Hotazel, Griquatown, and Kuruman IF in terms of $\delta^{65}Cu$ data,
375 is simply a manifestation of Cu having a common, isotopically homogeneous fine-grained
376 clastic provenance.

377 In an attempt to constrain further the source of Cu-bearing particulates in the investigated IF,
378 we have plotted spidergrams of the range and average transition metal abundances for each
379 IF normalised relative to the respective average data for arc tholeiite (Lodders and Fegley,
380 1998) (Fig. 8). We have included in our considerations corresponding average data and
381 compositional ranges for four stilpnomelane lutite samples from the Transvaal IF stratigraphy.
382 These lutites are commonly intercalated with the IF in distinct cm- to dm-thick layers, and are
383 widely considered to represent the lithified products of mixed chemical sedimentation with
384 contemporaneous episodes of volcanic ash deposition (Oonk, et al., 2017). We interpret the
385 comparably "flat" nature of all spidergrams with respect to all trace transition metals
386 (excepting Fe and Mn) as consistent with a common – albeit highly diluted in the case of IF –
387 volcanic ash source, especially for the three South African IF which are isotopically
388 indistinguishable in terms of their Cu isotopic signatures. Specifically, this signature recalls
389 that of igneous rocks, especially arc basalts (~0‰, Liu et al. (2015a)). We note that an anoxic
390 pre-GOE atmosphere and ocean would probably have been associated with lower dissolved
391 Cu river fluxes from continents because of sulphide stability and weaker break-down of
392 silicates with Cu in mafic rocks (e.g. pyroxenes) during weathering. In such case, the
393 particulate flux of Cu-bearing minerals would have been the relatively more dominant Cu

source to the global ocean at pre-GOE times, augmented by the simultaneous lack of plant cover on the continents (Martin and Whitfield, 1983).

The lack of Fe-Cu correlation in the present IF cores requires that the two elements followed different pathways. Iron in the Archean ocean is dominated by hydrothermal input (Thibon et al., 2019). In contrast, Cu in IF is dominated by a volcanogenic "detrital" component and, regardless of the residence time of Cu dissolved in the ocean, the output in the form of "chemical" Cu precipitated from the ocean is minor.

5. Conclusions and implications

The following points summarize the key results of the present study with regard to Cu and its isotopes in IF as a paleoceanographic proxy:

- Copper, and most other trace metals contained in IF, are present in vanishingly low concentrations by comparison to the bulk-rock iron content. They are also very low by comparison to transition metal contents in modern oceanic ferromanganese deposits and to the corresponding concentrations of average continental crust.
- The average δ^{65}Cu value of the Joffre IF is slightly negative (-0.24 ‰) but statistically invariant within analytical error. The good positive correlation between Cu and Ti abundances suggests that Cu and its isotopic signature in the Joffre IF most likely is derived from a terrigenous or volcanic detrital source and therefore is unrelated to water-column iron oxyhydroxide deposition.
- The average δ^{65}Cu data of all three of the South African IF (Kuruman, Griquatown, and Hotazel) are very close to 0 ‰ and are also essentially invariant within analytical error.

The average $\delta^{65}Cu$ values are thus independent of the relative age relationships of the three IF, pointing to no obvious oceanic reservoir effects related to Cu isotope fractionation through time.

- The $\delta^{65}Cu$ values of the South African IF are independent of first-order mineralogical variations from oxide- to carbonate-dominated assemblages (Kuruman-Griquatown IF). They are also independent of high bulk-rock Mn abundances and Mn/Fe ratios which characterise particularly the youngest Hotazel IF.
- Different associations between Cu and detritally-derived transition metals for the three South African IF and the Joffre IF of Australia, and correspondingly slight isotopic differences in average Cu isotope compositions, can most easily be interpreted as reflecting different sources of Cu-bearing particulates carrying a largely homogenous isotopic fingerprint in each case.

In view of our results and interpretations, we conclude that Cu and its stable isotope composition in IF are unsuitable records to reconstruct trends in redox evolution of the Archean-Proterozoic oceans and atmosphere, particularly with respect to the GOE. Iron formations are demonstrably poor reservoirs of primary oceanic Cu by comparison to Fe or Mn. They also record no apparent Cu isotope fractionation effects that could be linked to primary deposition of Fe or Mn oxhydroxides; instead, they reflect principally different provenance controls in the minor Cu-bearing particulate fraction of the primary sediments, likely derived from fine volcanic ash, probably of arc origin. The lack of any clear association between Cu and primary Fe and Mn oxyhydroxides may also lend support to recent studies suggesting that primary Fe (and Mn) precipitation in IF did not necessarily take place in the form of high-valence oxides and hydroxides, but chiefly in reduced mineral species such as greenalite (Johnson et al., 2018).

We consider it possible that other trace transition metals in IF are likely to suffer from exactly the same limitations that apply to Cu, especially when they are characterised by very low bulk-rock concentrations and erratic speciation behavior. We therefore propose that rigorous understanding of the trace metal speciation in IF is an imperative for the robust utility of corresponding bulk-rock concentration data and/or isotope ratios in paleoenvironmental studies.

Acknowledgments

We thank three anonymous referees and the Associate Editor, Olivier Rouxel, for constructive and insightful reviews. JBT acknowledges financial support from the Programme National de Planétologie (PNP) of the CNRS/INSU, co-funded by the CNES. We thank Philippe Telouk, Florent Arnaud-Godet, and Emmanuelle Albalat for occasional analytical assistance. The senior author, HT, is grateful to ENS de Lyon for having hosted him during part of winter 2019.

References

Albut, G., Babechuk, M.G., Kleinhanns, I.C., Benger, M., Beukes, N.J., Steinhilber, B., Smith, A.J.B., Kruger, S.J., Schoenberg, R. (2018) Modern rather than Mesoarchaean oxidative weathering responsible for the heavy stable Cr isotopic signatures of the 2.95 Ga old Ijzermijn iron formation (South Africa). *Geochimica et Cosmochimica Acta* **228**, 157-189.

Anbar, A.D., Duan, Y., Lyons, T.W., Arnold, G.L., Kendall, B., Creaser, R.A., Kaufman, A.J., Gordon, G.W., Scott, C., Garvin, J., Buick, R. (2007) A Whiff of Oxygen Before the Great Oxidation Event? *Science* **317**, 1903-1906.

462 Anbar, A.D., Rouxel, O. (2007) Metal Stable Isotopes in Paleoceanography. *Annual Review of Earth and*
463 *Planetary Sciences* **35**, 717-746.
464 Balistrieri, L.S., Borrok, D.M., Wanty, R.B., Ridley, W.I. (2008) Fractionation of Cu and Zn isotopes
465 during adsorption onto amorphous Fe(III) oxyhydroxide: Experimental mixing of acid rock drainage
466 and ambient river water. *Geochimica et Cosmochimica Acta* **72**, 311-328.
467 Calvert, S., Price, N. (1977) Geochemical variation in ferromanganese nodules and associated
468 sediments from the Pacific Ocean. *Marine Chemistry* **5**, 43-74.
469 Chi Fru, E., Rodríguez, N.P., Partin, C.A., Lalonde, S.V., Andersson, P., Weiss, D.J., El Albani, A.,
470 Rodushkin, I., Konhauser, K.O. (2016) Cu isotopes in marine black shales record the Great Oxidation
471 Event. *Proceedings of the National Academy of Sciences* **113**, 4941-4946.
472 Crowe, S.A., Dossing, L.N., Beukes, N.J., Bau, M., Kruger, S.J., Frei, R., Canfield, D.E. (2013) Atmospheric
473 oxygenation three billion years ago. *Nature* **501**, 535-538.
474 Danielson, A., Möller, P., Dulski, P. (1992) The europium anomalies in banded iron formations and the
475 thermal history of the oceanic crust. *Chemical Geology* **97**, 89-100.
476 Dekov, V.M., Rouxel, O., Asael, D., Hålenius, U., Munnik, F. (2013) Native Cu from the oceanic crust:
477 Isotopic insights into native metal origin. *Chemical Geology* **359**, 136-149.
478 Frei, R., Crowe, S.A., Bau, M., Polat, A., Fowle, D.A., Døssing, L.N. (2016) Oxidative elemental cycling
479 under the low O 2 Eoarchean atmosphere. *Scientific reports* **6**, 21058.
480 Frei, R., Gaucher, C., Døssing, L.N., Sial, A.N. (2011) Chromium isotopes in carbonates—a tracer for
481 climate change and for reconstructing the redox state of ancient seawater. *Earth and Planetary*
482 *Science Letters* **312**, 114-125.
483 Govindaraju, K. (1995) Update on two GIT-IWG geochemical reference samples: Albite from Italy, AL-
484 I and Iron Formation Sample from Greenland, IF-G. *Geostandards Newsletter* **19**, 55-96.
485 Gumsley, A.P., Chamberlain, K.R., Bleeker, W., Söderlund, U., de Kock, M.O., Larsson, E.R., Bekker, A.
486 (2017) Timing and tempo of the Great Oxidation Event. *Proceedings of the National Academy of*
487 *Sciences* **114**, 1811-1816.

Haugaard, R., Pecoits, E., Lalonde, S., Rouxel, O., Konhauser, K. (2016) The Joffre banded iron formation, Hamersley Group, Western Australia: Assessing the palaeoenvironment through detailed petrology and chemostratigraphy. *Precambrian Research* **273**, 12-37.

Heimann, A., Johnson, C.M., Beard, B.L., Valley, J.W., Roden, E.E., Spicuzza, M.J., Beukes, N.J. (2010) Fe, C, and O isotope compositions of banded iron formation carbonates demonstrate a major role for dissimilatory iron reduction in~ 2.5 Ga marine environments. *Earth and Planetary Science Letters* **294**, 8-18.

Johnson, J.E., Muhling, J.R., Cosmidis, J., Rasmussen, B., Templeton, A.S. (2018) Low-Fe(III) Greenalite Was a Primary Mineral From Neoarchean Oceans. *Geophysical Research Letters* **45**, 3182-3192.

Kendall, B., Reinhard, C.T., Lyons, T.W., Kaufman, A.J., Poulton, S.W., Anbar, A.D. (2010) Pervasive oxygenation along late Archaean ocean margins. *Nature Geoscience* **3**, 647-652.

Konhauser, K., Hamade, T., Raiswell, R., Morris, R., Ferris, F., Southam, G., E. Canfield, D. (2002) Could bacteria have formed the Precambrian banded iron formations? *Geological Society of America* **30**, 1079-1082.

Konhauser, K.O., Amskold, L., Lalonde, S.V., Posth, N.R., Kappler, A., Anbar, A. (2007) Decoupling photochemical Fe(II) oxidation from shallow-water BIF deposition. *Earth and Planetary Science Letters* **258**, 87-100.

Konhauser, K.O., Pecoits, E., Lalonde, S.V., Papineau, D., Nisbet, E.G., Barley, M.E., Arndt, N.T., Zahnle, K., Kamber, B.S. (2009) Oceanic nickel depletion and a methanogen famine before the Great Oxidation Event. *Nature* **458**, 750-753.

Konhauser, K.O., Planavsky, N.J., Hardisty, D.S., Robbins, L.J., Warchola, T.J., Haugaard, R., Lalonde, S.V., Partin, C.A., Oonk, P.B.H., Tsikos, H., Lyons, T.W., Bekker, A., Johnson, C.M. (2017) Iron formations: A global record of Neoarchaean to Palaeoproterozoic environmental history. *Earth-Science Reviews* **172**, 140-177.

512 Kurzweil, F., Wille, M., Gantert, N., Beukes, N.J., Schoenberg, R. (2016) Manganese oxide shuttling in
513 pre-GOE oceans – evidence from molybdenum and iron isotopes. *Earth and Planetary Science Letters*
514 **452**, 69-78.
515 Little, S., Sherman, D., Vance, D., Hein, J. (2014a) Molecular controls on Cu and Zn isotopic
516 fractionation in Fe–Mn crusts. *Earth and Planetary Science Letters* **396**, 213-222.
517 Little, S.H., Vance, D., Walker-Brown, C., Landing, W.M. (2014b) The oceanic mass balance of copper
518 and zinc isotopes, investigated by analysis of their inputs, and outputs to ferromanganese oxide
519 sediments. *Geochimica et Cosmochimica Acta* **125**, 673-693.
520 Liu, S.-A., Huang, J., Liu, J., Wörner, G., Yang, W., Tang, Y.-J., Chen, Y., Tang, L., Zheng, J., Li, S. (2015a)
521 Copper isotopic composition of the silicate Earth. *Earth and Planetary Science Letters* **427**, 95-103.
522 Liu, X.-M., Kah, L.C., Knoll, A.H., Cui, H., Kaufman, A.J., Shahar, A., Hazen, R.M. (2015b) Tracing Earth's
523 O2 evolution using Zn/Fe ratios in marine carbonates. *Geochemical Perspectives Letters* **2**, 23-34.
524 Lodders, K., Fegley, B. (1998). *The planetary scientist's companion*. Oxford University Press on
525 Demand.
526 Maréchal, C.N., Télouk, P., Albarède, F. (1999) Precise analysis of copper and zinc isotopic
527 compositions by plasma-source mass spectrometry. *Chemical Geology* **156**, 251-273.
528 Martin, J.-M., Whitfield, M. (1983) The significance of the river input of chemical elements to the
529 ocean, *Trace metals in sea water*. Springer, pp. 265-296.
530 Meng, Y., Bard, A.J. (2015) Measurement of Temperature-Dependent Stability Constants of Cu(I) and
531 Cu(II) Chloride Complexes by Voltammetry at a Pt Ultramicroelectrode. *Analytical Chemistry* **87**, 3498-
532 3504.
533 Millero, F.J. (2005). *Chemical Oceanography, Third Edition*. Taylor & Francis.
534 Oonk, P.B.H., Tsikos, H., Mason, P.R.D., Henkel, S., Staubwasser, M., Fryer, L., Poulton, S.W., Williams,
535 H.M. (2017) Fraction-specific controls on the trace element distribution in iron formations:
536 Implications for trace metal stable isotope proxies. *Chemical Geology* **474**, 17-32.

Ostrander, C.M., Nielsen, S.G., Owens, J.D., Kendall, B., Gordon, G.W., Romaniello, S.J., Anbar, A.D. (2019) Fully oxygenated water columns over continental shelves before the Great Oxidation Event. *Nature Geoscience* **12**, 186-191.

Partin, C., Lalonde, S.V., Planavsky, N., Bekker, A., Rouxel, O., Lyons, T., Konhauser, K. (2013) Uranium in iron formations and the rise of atmospheric oxygen. *Chemical Geology* **362**, 82-90.

Pickard, A.L. (2002) SHRIMP U-Pb zircon ages of tuffaceous mudrocks in the Brockman Iron Formation of Hamersley Range, Western Australia. *Australian Journal of Earth Sciences* **49**, 491-507.

Piper, D.Z., Williamson, M.E. (1977) Composition of Pacific Ocean ferromanganese nodules. *Marine Geology* **23**, 285-303.

Planavsky, N.J., Asael, D., Hofmann, A., Reinhard, C.T., Lalonde, S.V., Knudsen, A., Wang, X., Ossa Ossa, F., Pecoits, E., Smith, A.J.B., Beukes, N.J., Bekker, A., Johnson, T.M., Konhauser, K.O., Lyons, T.W., Rouxel, O.J. (2014) Evidence for oxygenic photosynthesis half a billion years before the Great Oxidation Event. *Nature Geosci* **7**, 283-286.

Posth, N.R., Hegler, F., Konhauser, K.O., Kappler, A. (2008) Alternating Si and Fe deposition caused by temperature fluctuations in Precambrian oceans. *Nature Geoscience* **1**, 703.

Rudnick, R.L., Gao, S. (2003) 3.01 - Composition of the Continental Crust A2 - Holland, Heinrich D, in: Turekian, K.K. (Ed.), *Treatise on Geochemistry*. Pergamon, Oxford, pp. 1-64.

Scott, C., Lyons, T.W., Bekker, A., Shen, Y., Poulton, S.W., Chu, X., Anbar, A.D. (2008) Tracing the stepwise oxygenation of the Proterozoic ocean. *Nature* **452**, 456-459.

Seward, T., Williams-Jones, A., Migdisov, A. (2014) 13.2 The Chemistry of Metal Transport and Deposition by Ore-Forming Hydrothermal Fluids, *Treatise on Geochemistry*. Elsevier Oxford, pp. 29-57.

Sheen, A.I., Kendall, B., Reinhard, C.T., Creaser, R.A., Lyons, T.W., Bekker, A., Poulton, S.W., Anbar, A.D. (2018) A model for the oceanic mass balance of rhenium and implications for the extent of Proterozoic ocean anoxia. *Geochimica et Cosmochimica Acta* **227**, 75-95.

562 Swanner, E.D., Planavsky, N.J., Lalonde, S.V., Robbins, L.J., Bekker, A., Rouxel, O.J., Saito, M.A., Kappler,
563 A., Mojzsis, S.J., Konhauser, K.O. (2014) Cobalt and marine redox evolution. *Earth and Planetary*
564 *Science Letters* **390**, 253-263.
565 Thibon, F., Blichert-Toft, J., Tsikos, H., Foden, J., Albalat, E., Albarede, F. (2019) Dynamics of oceanic
566 iron prior to the Great Oxygenation Event. *Earth and Planetary Science Letters* **506**, 360-370.
567 Tsikos, H., Beukes, N.J., Moore, J.M., Harris, C. (2003) Deposition, diagenesis, and secondary
568 enrichment of metals in the Paleoproterozoic Hotazel Iron Formation, Kalahari Manganese Field,
569 South Africa. *Economic Geology* **98**, 1449-1462.
570 Tsikos, H., Matthews, A., Erel, Y., Moore, J.M. (2010) Iron isotopes constrain biogeochemical redox
571 cycling of iron and manganese in a Palaeoproterozoic stratified basin. *Earth and Planetary Science*
572 *Letters* **298**, 125-134.
573 Von Damm, K.L. (1990) Seafloor hydrothemal activity : black smocker chemistry and chimneys. *Annual*
574 *Review of Earth and Planetary Sciences* **18**, 173-204.
575 Wang, X., Planavsky, N.J., Hofmann, A., Saupe, E.E., De Corte, B.P., Philippot, P., LaLonde, S.V., Jemison,
576 N.E., Zou, H., Ossa, F.O. (2018) A Mesoarchean shift in uranium isotope systematics. *Geochimica et*
577 *Cosmochimica Acta* **238**, 438-452.

578

579 **Figure captions**

580 Figure 1. Boxplots of (a) Mn/Fe x 10^2, (b) Cu/Fe x 10^6, and (c) δ^{65}Cu for each of the four IF of
581 this study (Joffre, Kuruman, Griquatown, and Hotazel). The pink line in (b) represents the
582 Cu/Fe ratio assumed in the oceanic Cu model of Chi Fru et al. (2016). Included for comparison
583 in (c) are the δ^{65}Cu data of pre- and post-GOE black shales from Chi Fru et al. (2016). These
584 boxplots represent the entire data range obtained for each IF, with the interquartile range

585 (between the 25th and 75th percentile) of the data defining the coloured areas, the lines
586 representing the corresponding median values, and the small black dots being outliers.

587 Figure 2. Correlation plots between Cu and trace metal concentrations of (a) Cr, (b) Ni, and
588 (c) V in the Transvaal IF; and (d) Ti in the Joffre IF. Joffre IF data include those from Chi Fru et
589 al. (2016).

590 Figure 3. Correlation plot between Cu and Fe concentrations in the Transvaal and Joffre IF.

591 Figure 4. Spidergram of average trace metal concentrations normalised relative to continental
592 crust (Rudnick and Gao, 2005) for all four IF of this study (Hotazel, Griquatown, Kuruman, and
593 Joffre). Included for comparison are compositional data for modern seawater (Millero, 2005),
594 manganese nodules (Calvert and Price, 1977; Piper and Williamson, 1977), and hydrothermal
595 fluids (Seward et al., 2014; Von Damm, 1990).

596 Figure 5. Color-coded Cu/Ti ratios of all IF samples (small circles) and corresponding averages
597 (large squares) obtained in this study, superimposed on the fields for IF (red), shale (green),
598 and continental crust (white line), as a function of geological time (modified after Chi Fru et
599 al. (2016)).

600 Figure 6. Fraction of Cu(I) chloride complexes at different chloride concentrations. The blue
601 vertical line represents the assumed concentration of chloride ions in the pre-GOE ocean.
602 Calculations done using the stability constant of Meng and Bard (2015).

603 Figure 7. Distribution of selected major elements and trace metals on a ternary diagram
604 depicting oxide, carbonate, and silicate fractions of IF from South Africa (adapted from Oonk
605 et al. (2017)).

606 Figure 8. Spidergram of the logarithm of average transition metal concentrations and ranges
607 (in grey), normalized to arc tholeiite (Lodders and Fegley, 1998) and assuming 0.7% TiO_2, for
608 all four IF of this study (Hotazel, Griquatown, Kuruman, and Joffre). Included for comparison
609 are corresponding compositional data and ranges (in purple) for stilpomelane lutite layers
610 from the Griquatown IF (Oonk et al., 2017).

611

612 **Table captions**

613 Table 1. Correlation coefficients between Cu and Cr, Ni, and V concentrations of the Transvaal
614 IF.

615

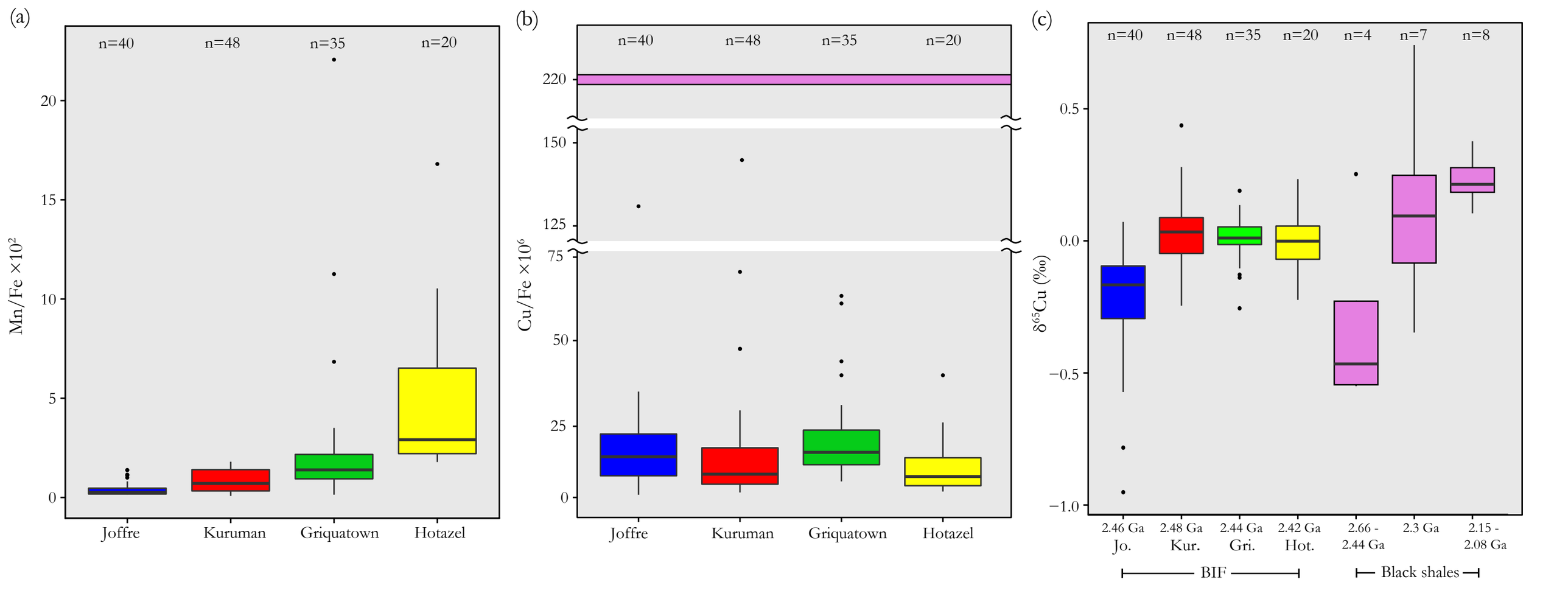
(a)
n=40
n=48
n=35
n=20
Mn/Fe ×10²
20
15
10
5
0
Joffre
Kuruman
Griquatown
Hotazel
(b)
n=40
n=48
n=35
n=20
Cu/Fe ×10⁶
220
150
125
75
50
25
0
Joffre
Kuruman
Griquatown
Hotazel
(c)
n=40
n=48
n=35
n=20
n=4
n=7
n=8
δ⁶⁵Cu (‰)
0.5
0.0
−0.5
−1.0
2.46 Ga
Jo.
2.48 Ga
Kur.
2.44 Ga
Gri.
2.42 Ga
Hot.
2.66 -
2.44 Ga
2.3 Ga
2.15 -
2.08 Ga
BIF
Black shales

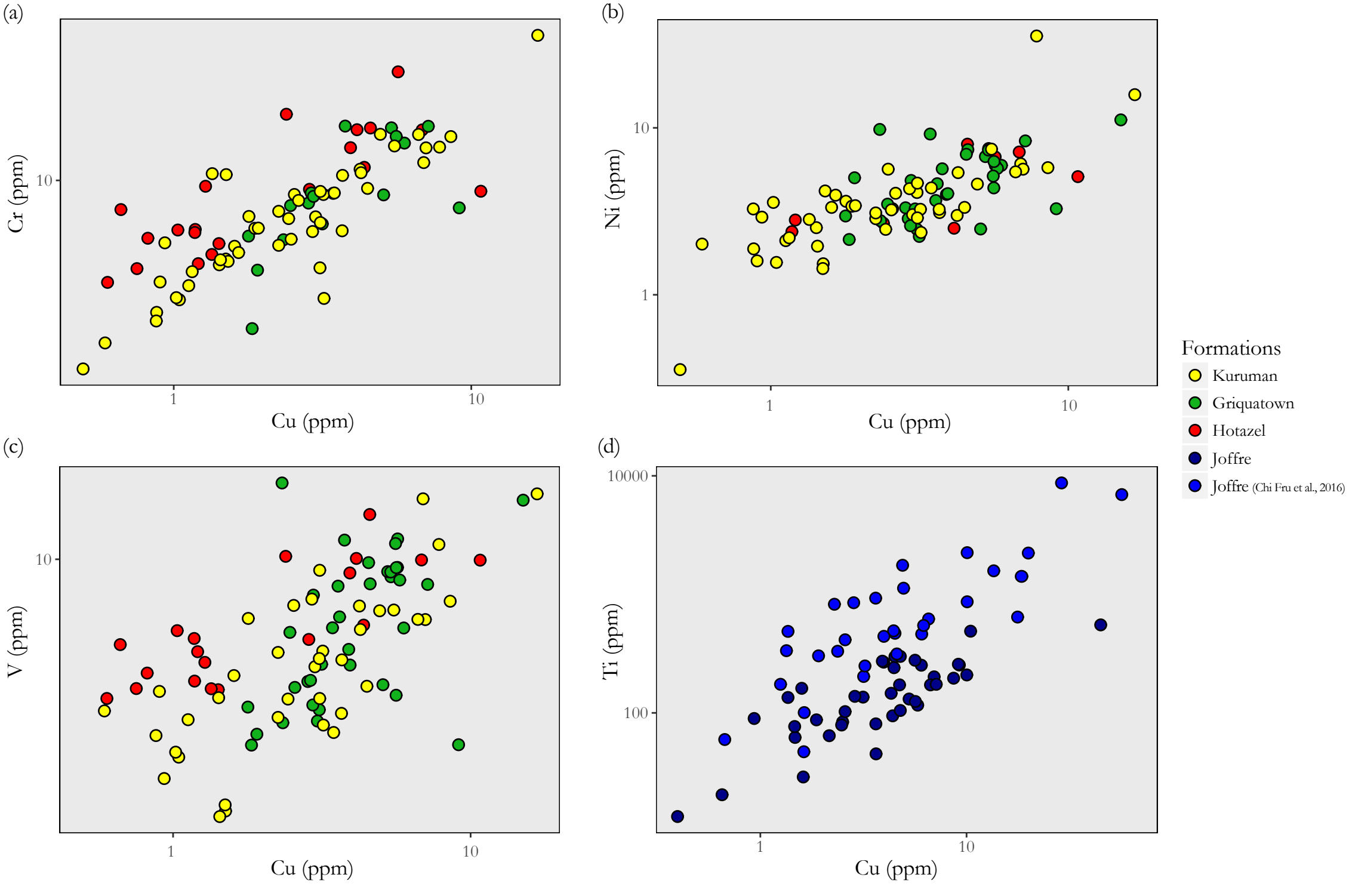
(a)
Cr (ppm)
10
1
10
Cu (ppm)
(b)
Ni (ppm)
10
1
1
10
Cu (ppm)
(c)
V (ppm)
10
1
10
Cu (ppm)
(d)
Ti (ppm)
10000
100
1
10
Cu (ppm)
Formations
Kuruman
Griquatown
Hotazel
Joffre
Joffre (Chi Fru et al., 2016)

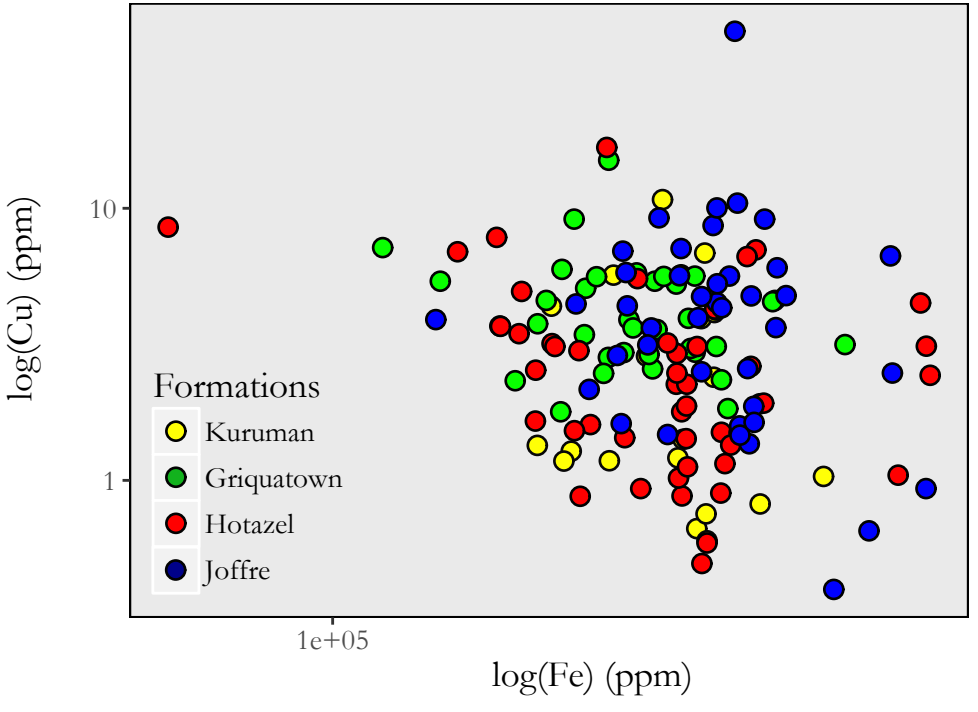
log(Cu) (ppm)
10
1
Formations
Kuruman
Griquatown
Hotazel
Joffre
1e+05
log(Fe) (ppm)

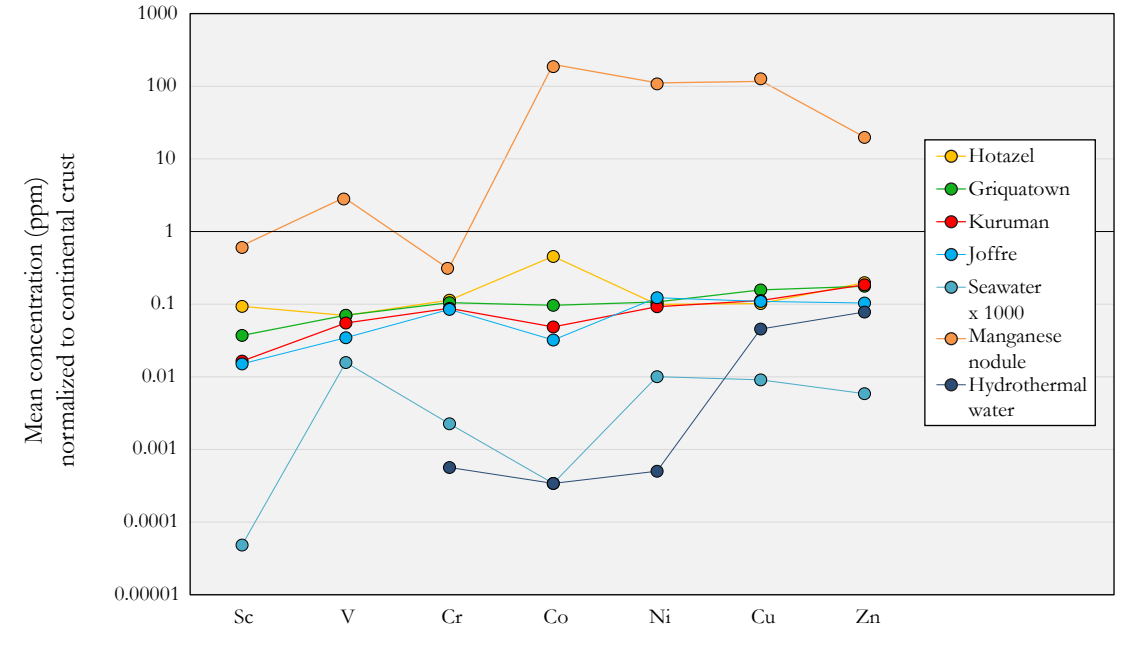
Mean concentration (ppm)
normalized to continental crust
1000
100
10
1
0.1
0.01
0.001
0.0001
0.00001
Sc
V
Cr
Co
Ni
Cu
Zn
Hotazel
Griquatown
Kuruman
Joffre
Seawater
x 1000
Manganese
nodule
Hydrothermal
water


Hotazel
Griquatown
Kuruman
Joffre
Joffre
(Chi Fru et al. 2016)
100
1
0.01
0.0001
molar Cu/Ti
3500
3000
2500
2000
1500
1000
500
0
Age (Ma)

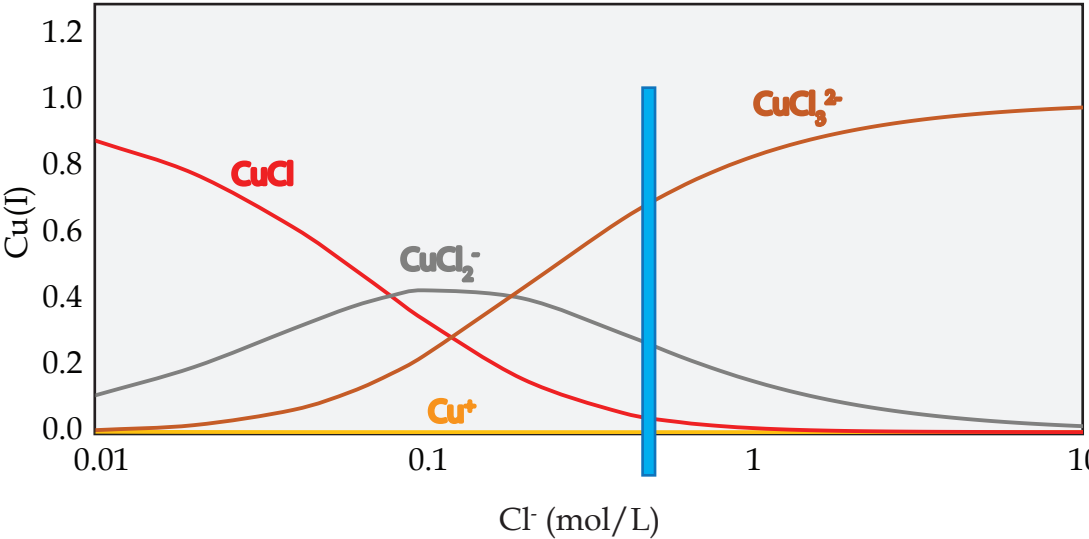
1.2
1.0
0.8
0.6
0.4
0.2
0.0
Cu(I)
CuCl
CuCl2-
CuCl3 2-
Cu+
0.01
0.1
1
10
Cl- (mol/L)

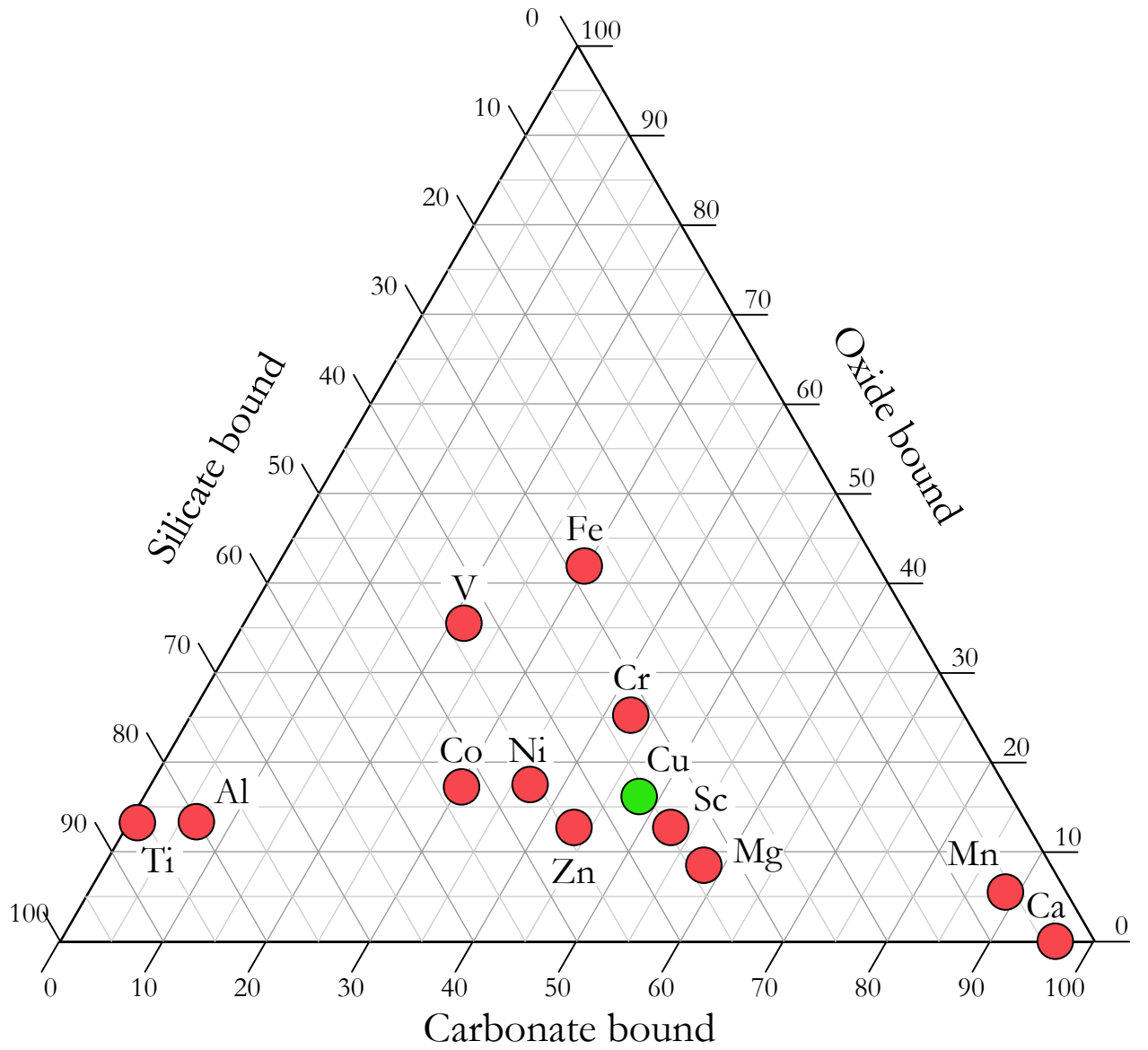
Silicate bound
Oxide bound
Carbonate bound
Fe
V
Cr
Co
Ni
Cu
Sc
Al
Ti
Zn
Mg
Mn
Ca

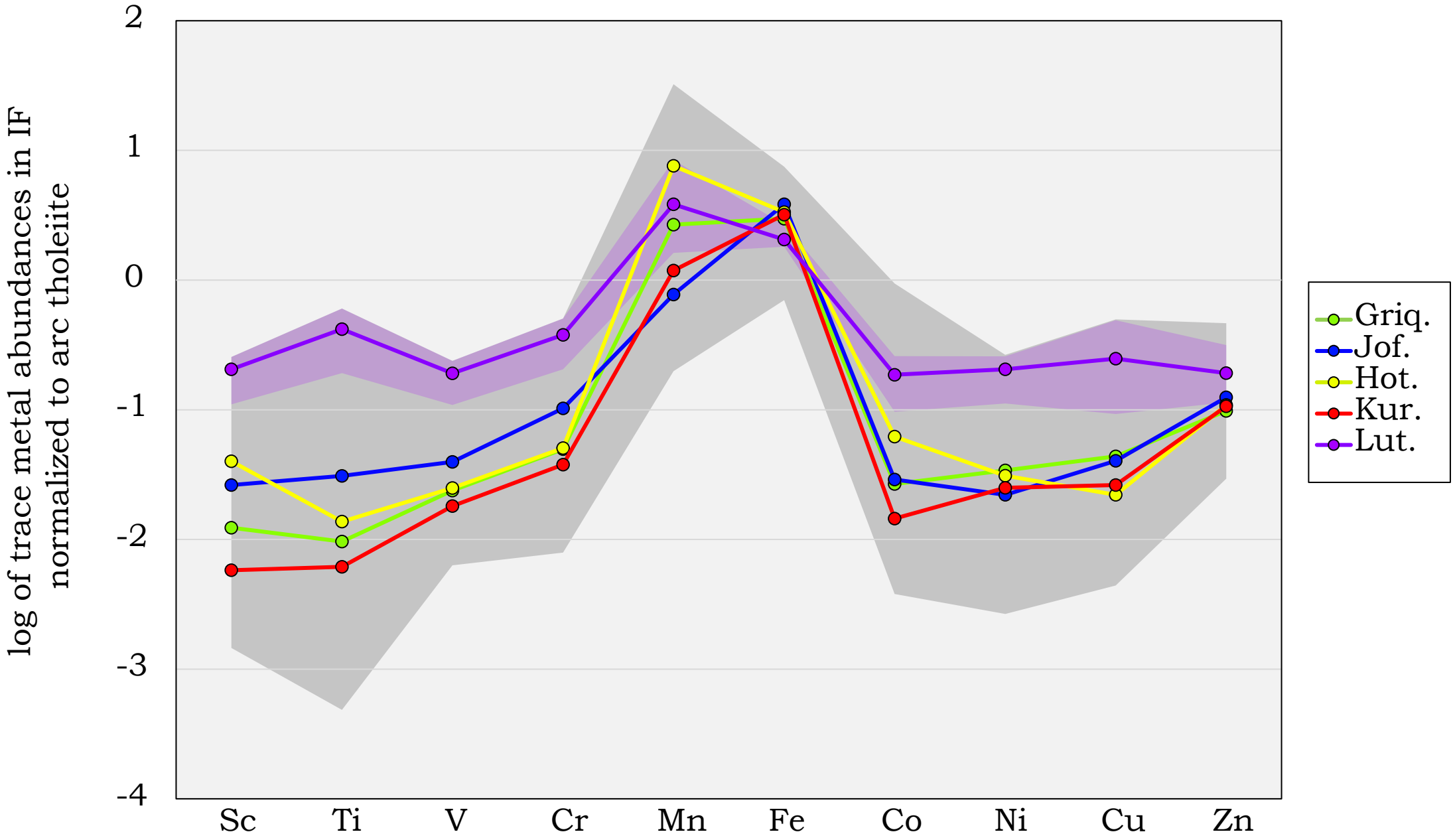
log of trace metal abundances in IF
normalized to arc tholeiite
2
1
0
-1
-2
-3
-4
Sc
Ti
V
Cr
Mn
Fe
Co
Ni
Cu
Zn
Griq.
Jof.
Hot.
Kur.
Lut.

	Cu-Cr	Cu-Ni	Cu-V
Hotazel	0.54	0.56	0.71
Griquatown	0.58	0.54	0.44
Kuruman	0.93	0.60	0.80